Human Molecular Genetics, 2014, Vol. 23, No. 6 ***1538–1550***
doi:10.1093/hmg/ddt541
Advance Access published on October 26, 2013

Mosaic synaptopathy and functional defects in Cav1.4 heterozygous mice and human carriers of CSNB2

Stylianos Michalakis[1], Lior Shaltiel[1], Vithiyanjali Sothilingam[2], Susanne Koch[1], Verena Schludi[1], Stefanie Krause[1], Christina Zeitz[3,4,5], Isabelle Audo[3,4,5,6,7], Marie-Elise Lancelot[3,4,5], Christian Hamel[8], Isabelle Meunier[8], Markus N. Preising[9], Christoph Friedburg[9], Birgit Lorenz[9], Nawal Zabouri[10], Silke Haverkamp[10], Marina Garcia Garrido[2], Naoyuki Tanimoto[2], Mathias W. Seeliger[2], Martin Biel[1] and Christian A. Wahl-Schott[1,*]

[1]Center for Integrated Protein Science Munich (CIPSM) and Department of Pharmacy—Center for Drug Research, Ludwig-Maximilians-Universität München, 81377 Munich, Germany [2]Division of Ocular Neurodegeneration, Institute for Ophthalmic Research, Centre for Ophthalmology, University of Tübingen, 72076 Tübingen, Germany [3]INSERM, UMR_S968, Paris F-75012, France [4]CNRS, UMR_7210, Paris F-75012, France [5]UPMC Univ Paris 06, UMR_S 968, Institut de la Vision, Paris F-75012, France [6]Centre Hospitalier National d'Ophtalmologie des Quinze-Vingts, INSERM-DHOS CIC 503, Paris F-75012, France [7]UCL-Institute of Ophthalmology, London EC1V 9EL, UK [8]CHRU, Genetics of Sensory Diseases, Montpellier 34091, France [9]Department of Ophthalmology, Justus-Liebig-University Giessen, Universitätsklinikum Giessen and Marburg GmbH, Giessen Campus, 35392 Giessen, Germany [10]Neuroanatomy, Max-Planck-Institute for Brain Research, 60438 Frankfurt/M, Germany

Received September 6, 2013; Revised and Accepted October 24, 2013

Mutations in *CACNA1F* encoding the α_1-subunit of the retinal Cav1.4 L-type calcium channel have been linked to Cav1.4 channelopathies including incomplete congenital stationary night blindness type 2A (CSNB2), Åland Island eye disease (AIED) and cone-rod dystrophy type 3 (CORDX3). Since *CACNA1F* is located on the X chromosome, Cav1.4 channelopathies are typically affecting male patients via X-chromosomal recessive inheritance. Occasionally, clinical symptoms have been observed in female carriers, too. It is currently unknown how these mutations lead to symptoms in carriers and how the retinal network in these females is affected. To investigate these clinically important issues, we compared retinal phenotypes in Cav1.4-deficient and Cav1.4 heterozygous mice and in human female carrier patients. Heterozygous *Cacna1f* carrier mice have a retinal mosaic consistent with differential X-chromosomal inactivation, characterized by adjacent vertical columns of affected and non-affected wild-type-like retinal network. Vertical columns in heterozygous mice are well comparable to either the wild-type retinal network of normal mice or to the retina of homozygous mice. Affected retinal columns display pronounced rod and cone photoreceptor synaptopathy and cone degeneration. These changes lead to vastly impaired vision-guided navigation under dark and normal light conditions and reduced retinal electroretinography (ERG) responses in *Cacna1f* carrier mice. Similar abnormal ERG responses were found in five human *CACNA1F* carriers, four of which had novel mutations. In conclusion, our data on Cav1.4 deficient mice and human female carriers of mutations in *CACNA1F* are consistent with a phenotype of mosaic CSNB2.

*To whom correspondence should be addressed at: Department Pharmazie, Pharmakologie für Naturwissenschaften, Ludwig-Maximilians-Universität München, Butenandtstr. 5-13, D-81377 München, Germany. Tel: +49 89218077654; Fax: +49 89218077326; Email: christian.wahl@cup.uni-muenchen.de

INTRODUCTION

Retinal photoreceptors and bipolar cells contain a highly specialized type of synapse designated ribbon synapse (1,2). Neurotransmitter release in these synapses is controlled via graded and sustained changes in membrane potential that are maintained throughout the duration of a light stimulus. Cav1.4 L-type Ca^{2+} channels are the main channel subtype converting these analog input signals into corresponding tonic glutamate release (3–6). Cav1.4 channels are tailored to this function since they display very slow voltage-dependent inactivation (VDI) and a lack of Ca^{2+}-dependent inactivation (CDI). Cav1.4 channels are multisubunit complexes consisting of the principal α_1 and the auxiliary β_{2a} and $\alpha 2\delta$ subunits (3,7). The α_1 subunit of retina-specific Cav1.4 voltage-gated L-type calcium channels is encoded by the X-chromosomal *CACNA1F* gene. Mutations in *CACNA1F* have been identified in patients suffering from congenital stationary night blindness type 2 (CSNB2; incomplete X-linked CSNB; OMIM: 300 071) (8,9), Åland Island eye disease (AIED; OMIM: 300 600) (10,11) and X-linked cone-rod dystrophy (CORDX3; OMIM: 300 476) (12). These channelopathies display similar electroretinographic changes that indicate a loss of neurotransmission from rods to bipolar cells, which is consistent with a loss of Cav1.4 function in rod photoreceptor synapses. In addition, some patients present with varying degrees of cone photoreceptor impairments. Deletion of Cav1.4 in mice leads to profound visual impairment. These mice also seem to have a variable phenotype but in general a more severe phenotype than human patients (13–16).

Cav1.4 channelopathies are transmitted by X-chromosomal inheritance. Therefore, males are affected far more frequently than females. Clinical symptoms have occasionally been observed also in carrier females (17,18). Interestingly, the c.2234T>C, p.Ile745Thr *CACNA1F* mutation (17,19) revealed a severe retinal phenotype in a large New Zealand family with male children showing abnormal color vision and reduced intellectual abilities. More importantly, female carriers presented with abnormal ERGs. The authors argued that the presence of symptoms in female carriers may relate to the specific mutation which results in increased, rather than loss of, activity of the Cav1.4 calcium channel. A mouse model for this particular mutation has been described (14), but the phenotypes of males and females have not yet been reported.

In the present study, we set out to further explore the phenotype observed in female carriers of loss of function mutation in *CACNA1F*. To this end, we addressed this clinically important issue by a comparative analysis of retinal phenotypes in Cav1.4 deficient and Cav1.4 heterozygous mice and compared these results to the clinical information obtained from human female carriers presenting with four novel mutations in *CACNA1F*.

RESULTS

Retinal and visual function in Cav1.4 deficient mice

In the wild-type retina, Cav1.4 protein localizes to rod and cone photoreceptor synapses within the outer plexiform layer (opl) and to a lesser extent to rod bipolar cell synapses in the inner plexiform layer (ipl) (Fig. 1A). In retinas from Cav1.4 deficient

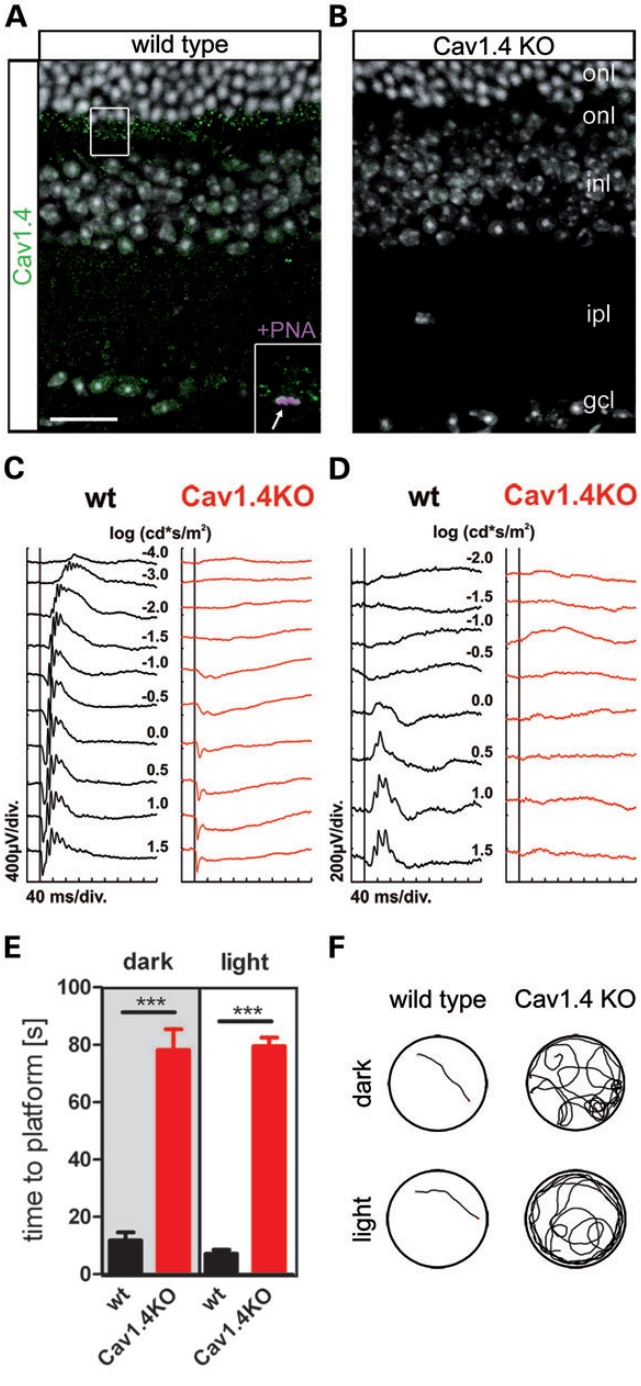

Figure 1. Visual function in *Cacna1f*- knockout mice. (**A** and **B**) Confocal scans of vertical retinal sections from wild-type (A) and *Cacna1f* knockout (Cav1.4-KO) mice (B) labeled with a Cav1.4-specific antibody (green). Cell nuclei were stained with the nuclear dye Hoechst 33342 (grey). Inlay in (A): magnification view on the outer plexiform layer (opl) region marked with a white rectangle illustrating the partial co-localization of the Cav1.4 signal (green) with the cone pedicle marker peanut agglutinin (PNA, magenta). (**C** and **D**) Electroretinographic analysis of retinal function in Cav1.4-KO mice. Representative Ganzfeld-ERG intensity series from dark-adapted (C) and light-adapted (D) wild-type (wt, black traces) and Cav1.4-KO mice (red traces). (**E** and **F**) Performance of Cav1.4-KO mice in a visual water-maze behavioral task. (E) Latency to locate a visible platform under dark (left two bars) and normal light conditions (right two bars). (F) Example swimming paths under dark (upper part) and normal light conditions (lower part). The scale bar marks 20 µm. gcl, ganglion cell layer; inl, inner nuclear layer; ipl, inner plexiform layer; onl, outer nuclear layer.

(Cav1.4-KO) mice (14), Cav1.4 immunoreactivity was not longer present in the opl and the ipl (Fig. 1B). Most immunoreactivity observed in the opl of wild-type retina corresponds to rod photoreceptor synapses. However, double labeling with the cone pedicle marker peanut agglutinin (PNA) revealed that cone photoreceptor synapses are also Cav1.4 immunopositive (Fig. 1A inlay).

The overall retinal function of Cav1.4-KO mice was evaluated by Ganzfeld Electroretinography (ERG) using stimulation protocols to isolate rod- (Fig. 1C) or cone-driven (Fig. 1D) light responses. In the dark-adapted (scotopic) part of the protocol, in which cones are non-responsive, the b-wave component and oscillatory potentials were completely absent in ERG recordings of Cav1.4-KO mice when compared with wild-type mice throughout the stimulus range (Fig. 1C). However, the amplitude and the threshold of the a-wave in Cav1.4-KO mice were similar to wild-type. In the light-adapted (photopic) part of the ERG, in which rods are non-responsive due to desensitization, the b-wave component and oscillatory potentials were also completely absent in Cav1.4-KO mice (Fig. 1D). The absence of a scotopic and photopic b-wave in the Cav1.4-KO mice is consistent with a defect in neurotransmission from both rod and cone photoreceptors to second-order neurons, particularly bipolar cells.

The functional significance of the observed defects in the ERG responses was evaluated by testing the visual performance of Cav1.4-KO mice in a vision-guided water-maze behavioral task. The latency to navigate to a visible platform under dark and normal light conditions was significantly increased in Cav1.4-KO when compared with wild-type mice (Fig. 1E). Moreover, in 37.5 $\pm$ 9.1% of the trials in the dark and 27.3 $\pm$ 4.4% of the trials during light Cav1.4-KO mice did not manage to find the platform within the test period of 2 min (scored as error of omission). In contrast all wild-type mice reached the platform within time in all test trials. Wild-type mice dramatically improved their visual performance on day 2 to a maximum, which could not be further improved during the third test day under dark light conditions (Supplementary Material, Fig. S2A). Under normal light conditions (day four) no further improvement was observed (Supplementary Material, Fig. S2A). In contrast to wild-type mice, Cav1.4-KO mice struggled to locate the platform and showed no improvement during the three successive test days under dark or on the fourth test day under normal light conditions. Consistent with the increased latency of Cav1.4-KO mice the swimming path was much longer (Fig. 1F). To exclude that residual cone function could not be detected in this test paradigm in Cav1.4-KO mice, we tested another group of animals for three consecutive days solely under normal light conditions. Again, wild-type mice displayed a robust learning curve, whereas Cav1.4-KO mice did not show any improvement (Supplementary Material, Fig. S2B), confirming that cone function is also strongly compromised in Cav1.4-KO mice.

Synaptopathy in Cav1.4 deficient mice

Having characterized the functional defects in Cav1.4-KO mice, we set out to analyze the changes of the retinal network architecture of Cav1.4-KO mice at the morphological level. It is well established that second order retinal neurons, e.g. bipolar cells (BC) and horizontal cells (HC) respond to a number of pathological conditions by extending sprouting processes into the outer nuclear layer (onl) (20–23). Staining of wild-type retinas for the horizontal and amacrine cell marker calbindin showed strong labeling of horizontal cell bodies and a dense plexus of horizontal cell processes in the opl (Fig. 2A). In contrast, in retinas of Cav1.4-KO mice calbindin staining was reduced in the opl and numerous elongated horizontal cell neurites extended far into the outer nuclear layer (onl) (Fig. 2B). This phenomenon was also observed in aged animals (Fig. 2C) confirming that it is not restricted to certain age periods. In wild-type retinas, stainings by PKCα, a rod bipolar cell marker, displayed regular arborization of bipolar cell dendrites restricted to the opl (Fig. 2D). In contrast, in retinas of Cav1.4-KO mice, rod bipolar cell dendrites extended beyond the opl, far into the onl (Fig. 2E). Moreover, the staining revealed compromised morphology of rod BC synapses in the ipl of Cav1.4-KO mice (Fig. 2D and E). The PKCα antibody also labels cone outer segments (upper part in Fig. 2D and E), which appear disorganized in Cav1.4-KO mice. The irregular outgrowth of HC and BC neurites concurred with a marked thinning of the opl in Cav1.4-KO retinas when compared with wild-type retina. This was particularly evident in retinal slices stained with the nuclear dye Hoechst 33342 as thinning of the gap between the outer and inner nuclear layers (Fig. 2A–C).

Together, these findings indicate disturbed synaptic contacts between photoreceptors and second order neurons. We therefore performed a set of stainings to evaluate the distribution of presynaptic markers in the Cav1.4-KO retina. The vesicular glutamate transporter 1 (vGlut1) labels rod spherules and cone pedicles in the opl as well as axon terminals of bipolar cells in the ipl (24). The complexins (Cplx) 3 and 4 label cone pedicles or rod and cone synapses, respectively (25). Stainings for vGlut1 (Fig. 2F and G), Cplx3 and Cplx4 (Fig. 2H–K) confirmed a greatly reduced immunoreactivity in the opl and an increased punctuate staining in the onl in Cav1.4-KO mice when compared with wild-type control mice. These results are consistent with a retraction of photoreceptor synapses from the opl into the onl. In addition, the vGlut1 staining revealed a markedly reduced labeling of rod BC synapses in the knockout (Fig. 2F and G), which is in line with the reduction of PKCα stainings in rod BC synapses of Cav1.4-KO mice (Fig. 2E).

Cone photoreceptor degeneration in Cav1.4 deficient mice

We next analyzed whether the severe synaptic pathology is associated with additional changes of photoreceptor morphology. To this end, we labeled wild-type and knockout retinas with rod and cone photoreceptor markers. The rod phototransduction cascade protein rod arrestin (also known as visual arrestin or S-antigen) revealed similar expression and localization in outer segments of wild-type and mutant retinas (Fig. 3A and B). However, the synaptic fraction of rod arrestin labeling (arrows in Fig. 3A) was lost from the opl and partially found in the onl (arrows in Fig. 3B). In contrast, labeling of Cav1.4-KO retinas for the cone photoreceptor-specific homologue cone arrestin revealed a loss of immunosignal compared with wild-type mice (Fig. 3C and D). Specific labeling of cone photoreceptor extracellular matrix by peanut agglutinin (PNA) revealed a loss of cone pedicles in the opl while the morphology of the cone inner and outer segments was normal (Fig. 3E and F).

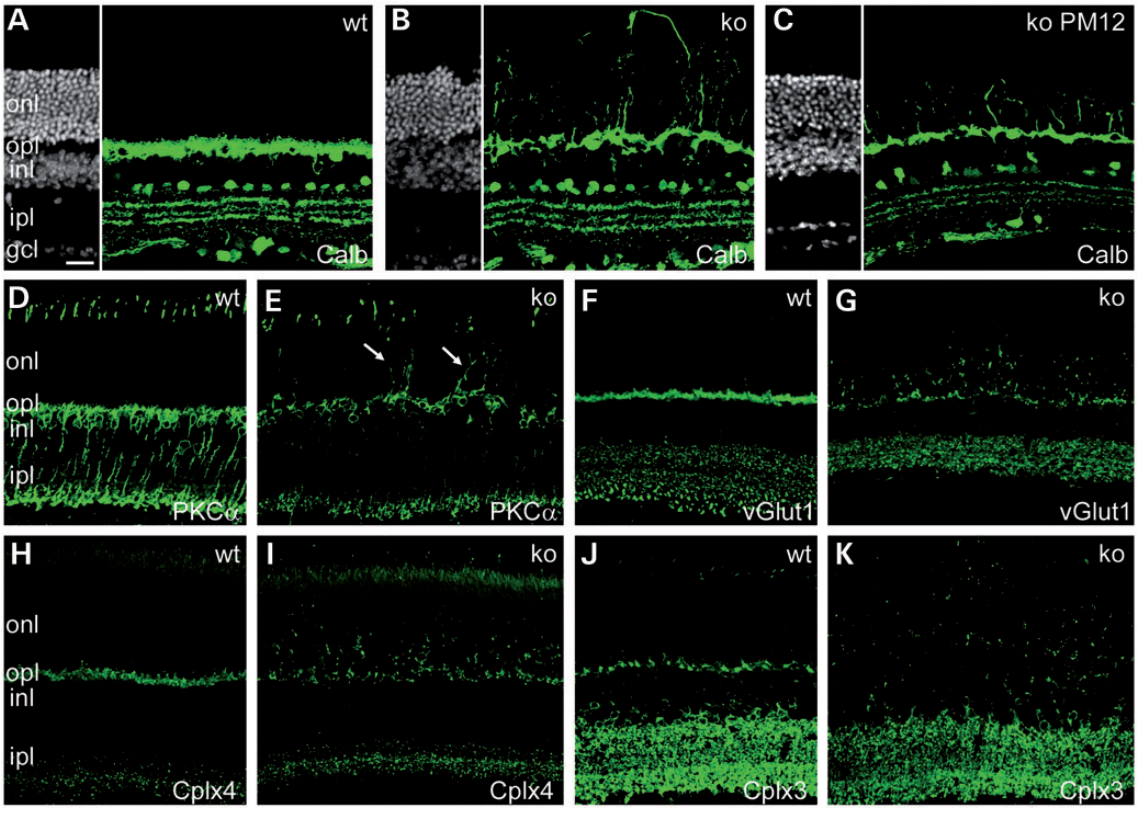

Figure 2. Synaptic changes in *Cacna1f* deficient mice. Confocal scans of vertical retinal sections from wild-type (wt) and Cav1.4-KO (ko) mice. (**A**–**C**) Immunolabeling of horizontal and amacrine cells with calbindin (Calb, green, right parts in A–C). The cell nuclei were stained with the dye Hoechst 33342 (grey) to illustrate the retinal layers (left part in A–C). Horizontal cell neurites extend deep into the outer nuclear layer (onl) in young (6-week-old) (B) and aged (12-month-old, PM 12) ko mice (C). (**D** and **E**) Retinal sections from 6-week-old wt and ko mice immunolabeled with the rod bipolar cell marker protein kinase C alpha (PKCα) (D and E), as well as with the presynaptic markers vesicular glutamate transporter 1 (vGlut1) (**F** and **G**), complexin 4 (Cplx4) (**H** and **I**) and complexin 3 (cplx3) (**J** and **K**). PKCα staining demonstrates pronounced growth of rod bipolar cell dendrites into the onl of Cav1.4-KO mice (arrows in E). Note that PKCα also labels cone outer segments (upper part in D and E), which appear disorganized in the ko (E). The presynaptic markers (F–K) also reveal a disperse redistribution of rod (vGlut1 and Cplx4) and cone (Cplx3) presynaptic elements from the outer plexiform layer (opl) to the onl in the ko (G, I and K). inl, inner nuclear layer; ipl, inner plexiform layer. The scale bar shown in (A) marks 20 μm.

In order to examine whether down-regulation of cone arrestin reflected ongoing cone degeneration, we labeled wild-type and Cav1.4-KO retinas for the Müller glial cell-specific glial fibrillary acid protein (GFAP). In wild-type retina GFAP is only found in Müller glial cell endfeet (Fig. 3G). In contrast, strongly GFAP-positive stress fibers appear in Müller glial cells of Cav1.4-KO mice (Fig. 3H) indicating the presence of a reactive gliosis. A similar reactive gliosis can also be observed in classical mouse models of cone degeneration (21,26).

Together these findings indicate that the synaptopathy in the Cav1.4-KO mouse has no obvious effect on rod outer segment morphology, but is associated with an overall compromised cone photoreceptor morphology and cone degeneration.

Morphological changes in Cav1.4 heterozygous mice (carriers)

Having defined the morphological changes in the Cav1.4-KO retina, we next set out to study whether morphological changes are also present in heterozygous female mice (Cav1.4$^{+/-}$). Distribution of Cav1.4 protein was patchy, characterized by islets of Cav1.4 immunoreactivity and areas without Cav1.4 immunoreactivity next to each other (Fig. 4A–C).

To test the hypothesis that this could result in mosaic synaptic defects in heterozygous mice, we stained for calbindin (Fig. 4D–F), vGlut1 (Fig. 4G–I) and complexin 3 (Fig. 4J–L). This revealed a similar patchy pattern of changes in synaptic morphology. Specifically, retinal network columns with compromised morphology were radially oriented and displayed outgrowths of horizontal cell neurites and bipolar cell dendrites into the onl and thinning of the opl, whereas neighboring non-affected network columns revealed wild-type-like appearance (Fig. 4D–L). Moreover, in affected Cav1.4-KO-like retinal columns of the heterozygous retina, we also observed a loss of cone pedicles (Fig. 4M), down-regulation of cone arrestin (Fig. 4N) and reactive gliosis (Fig. 4O).

We next wondered how the synaptic contacts between photoreceptors and second order neurons are organized in Cav1.4 heterozygous mice, in particular at the border regions between healthy and affected retina. We therefore analyzed retinal slices double-labeled with specific pre- and postsynaptic markers. Figure 5A–C shows images for PKCα and Ctbp2 (Fig. 5A). Ctbp2 is a marker of the photoreceptor synaptic ribbon and labels characteristic horseshoe-shaped structures in rod and cone photoreceptor synapses (27). While Ctbp2 is still expressed in the Cav1.4-KO (data not shown) and in affected

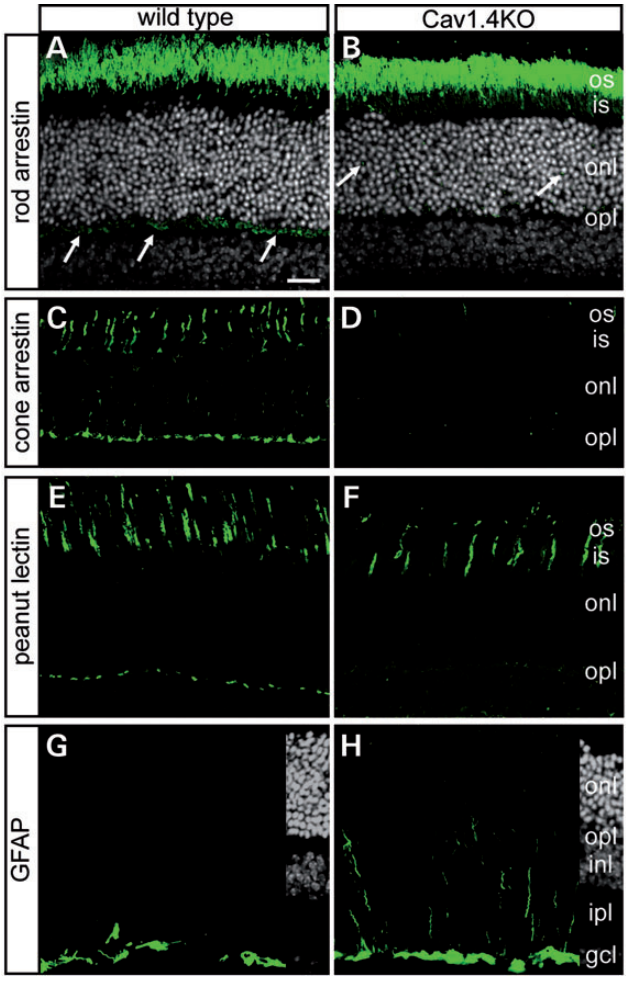

Figure 3. Photoreceptor morphology in *Cacna1f* deficient mice. Confocal scans of vertical retinal sections from 6-week-old wild-type and Cav1.4-KO mice labeled for rod arrestin (**A** and **B**), cone arrestin (**C** and **D**), peanut agglutinin (**E** and **F**) and GFAP (**G** and **H**). (A and B) The outer segment expression and localization of rod arrestin is not compromised in the KO. However, the synaptic fraction of rod arrestin labeling (arrows in A) was lost from the outer plexiform layer (opl) and was partially found in the outer nuclear layer (onl) (arrows in B). Cell nuclei were stained with the nuclear dye Hoechst 33342 (grey). (C and D) Cone arrestin is markedly downregulated throughout the cone cells in the KO (D). (E and F) Peanut lectin staining of cone photoreceptor extracellular matrix reveals a loss of cone pedicles, but preservation of cone inner and outer segment (is, os) morphology. (G and H) Induction of GFAP-positive stress fibers in the KO retina. Right part in panels (G and H) are Hoechst 33342 (grey) images of the respective retinal slices. The scale bar marks 20 μm. gcl, ganglion cell layer; inl, inner nuclear layer; ipl, inner plexiform layer; onl, outer nuclear layer.

parts of the Cav1.4$^{+/-}$ retina (Fig. 5A), the normal signal is decreased in the opl and appears redistributed throughout the onl. Other presynaptic markers relocate similarly (e.g. vGlut1). Interestingly, most of the ectopic Ctbp2 signal in the affected area also had aberrant morphology (Fig. 5B and C). However, ectopic Ctbp2 staining in the onl that was in close proximity to PKCα-positive rod BC dendrite, have an appearance similar to the Ctbp2 signal in the wild-type (data not shown) or healthy parts of the opl in the heterozygous retina (Fig. 5C). Another pair of pre- and postsynaptic markers that we analyzed was vGlut1 and the Cav1.1 voltage-gated L-type calcium channel α_1 subunit (also known as Cacna1 s) (Fig. 5D and E). Cav1.1 localizes to ON BC dendrites in the wild-type and in the non-affected part of the Cav1.4 heterozygous retina (Fig. 5D). In contrast, it is strongly down-regulated in the Cav1.4-KO (14) and the affected part of the Cav1.4 heterozygous retina (Fig. 5D). Interestingly, ectopic Cav1.1 signal could also be seen throughout the onl in the border region between affected and healthy areas of the Cav1.4 heterozygous retina (Fig. 5D and E) suggesting the formation of ectopic synapses between ON BCs within affected retinal columns lacking normal input and neighboring non-affected photoreceptors (Fig. 8).

Functional changes in Cav1.4 heterozygous mice (carriers)

We next assessed the retinal function in Cav1.4$^{+/-}$ mice in analogy to Cav1.4-KO mice. Scotopic ERGs were characterized by reduced b-wave amplitudes and, superimposed on them, oscillatory potentials throughout the stimulus range in the carrier mice when compared with the wild-type (Fig. 6A and B). However, the threshold of the b-wave as well as the amplitude and the threshold of the a-wave were normal in Cav1.4$^{+/-}$ mice. A similar reduction in the b-wave amplitude was also observed for the photopic ERGs (Fig. 6C and D). These findings are characteristic for a functional defect in the transmission of visual signals from rod and cone photoreceptors to bipolar cells in Cav1.4$^{+/-}$ mice.

We also tested whether this impaired retinal processing had any influence on the ability of Cav1.4$^{+/-}$ mice to navigate in a visual water maze. Indeed, the performance of Cav1.4$^{+/-}$ mice under dark conditions was in between the wild-type and Cav1.4-KO mice (Fig. 6E and F), as judged by both, the latency to locate the platform (Fig. 6E) and the errors to find the platform during the trial (errors of omission) (Fig. 6F). Under normal light conditions the phenotype was somewhat milder since heterozygous mice had only slightly increased latencies and did not make any error of omissions (Fig. 6G and H).

CACNA1F mutations and phenotypes in male patients and female carriers

Given the morphological and functional defects in Cav1.4$^{+/-}$ carrier mice, we investigated visual function and morphology in five females carrying *CACNA1F* mutations from families seen by two different clinical centers (Fig. 7; Supplementary Material, Fig. S3). Four of the mutations were novel. The mutation spectrum comprised two missense mutations in exons 6 and 16 (c.764G>A, p.Gly255Glu and c.2090T>C, p.Leu697Pro), which are predicted to cause exchanges of amino acid residues in transmembrane segment S5 of domain I (p.Gly255Glu) and in the pore loop of domain II (p.Leu697Pro). In addition, three mutations were identified, which were predicted either to result in mRNA decay or in a truncated Cav1.4 channel protein: In the mutation (c.2821dupC, p.Leu941Profs*115) a duplication in exon 23 is predicted to cause a frameshift at amino acid residue 941 (segment S3 of domain III), which changes the 115 following amino acid residues. After these 115 residues the protein is truncated. In the mutation (c.4547_4549delinsCC, p.Leu1516Profs*9), a deletion/insertion in exon 39 is predicted to cause a frameshift at the amino acid residue 1516 (proximal

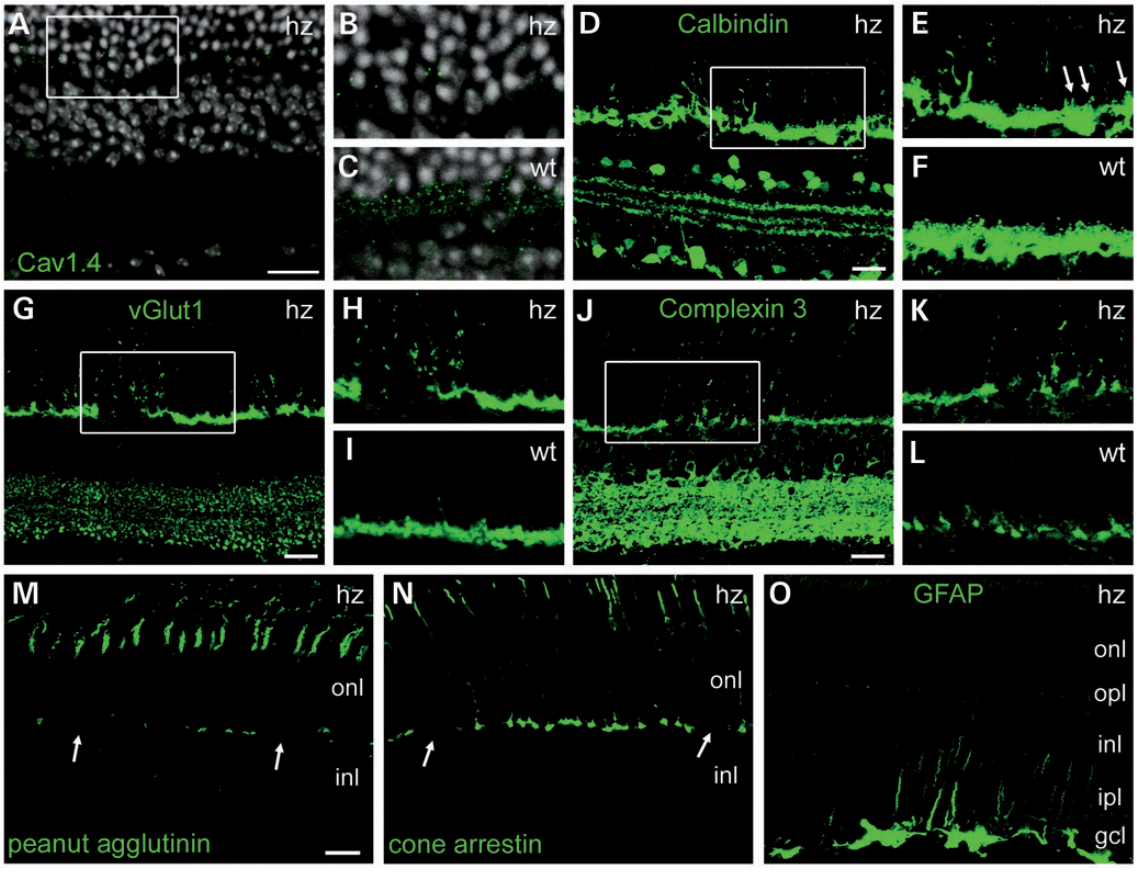

Figure 4. Mosaic synaptopathy in *Cacna1f* heterozygous mice. Confocal scans of vertical retinal sections from Cav1.4 heterozygous (hz) mice. (**A**) Representative image from an hz mouse labeled with a Cav1.4-specific antibody (green). (**B**) Magnification view on the outer plexiform layer region marked with a white rectangle in (A). (**C**) Magnification view on the corresponding region from a wild-type control mouse labeled with a Cav1.4-specific antibody (green). Cell nuclei in (A–C) were stained with the nuclear dye Hoechst 33342 (grey). (**D**–**L**) Retinal sections from hz (D and E, G and H and J–H) and wt (F, I and L) mice immunolabeled for calbindin (Calb, D–F), vGlut1 (G–I) and complexin 3 (cplx3) (J–L). The hz mice show a pronounced mosaic (patchy) photoreceptor synaptopathy. The regions marked with a white rectangle in panels (D, G and J) are shown in (E, H and K), respectively. (F, I and L) show corresponding immunostainings from wt. (**M**–**O**) Representative image from hz mice labeled for peanut agglutinin (M), cone arrestin (N) and GFAP (O) reveal a mosaic loss of synaptic cone structures and reactive gliosis in the hz. The scale bar marks 20 μm. gcl, ganglion cell layer; inl, inner nuclear layer; ipl, inner plexiform layer; onl, outer nuclear layer; opl, outer plexiform layer.

C-terminus), which changes the nine following amino acid residues. After these nine residues, the protein is truncated. Mutation c.2928+1G>A has been reported before (IVS24+1) (28). The location of the mutations in the Cav1.4 channel protein is shown in Supplementary Material, Figure S3.

All carriers showed visual abnormalities of variable extent (Table 1). Importantly, all carriers had a variable degree of ERG changes (Fig. 7). While rod function reached the lower normal range in some, cone function never reached more than half the normal size (Fig. 7, Table 1). The clinical symptoms and the pathological ERG changes of carrier females were consistent with the phenotype of incomplete CSNB. This phenotype co-segregated in affected male patients and was present at the heterozygous state in all female carriers (Table 1, Fig. 7).

DISCUSSION

Neurotransmission from photoreceptors to bipolar cells relies on calcium-triggered release of glutamate from photoreceptor synaptic terminals (1,2). The major calcium entry pathway in presynaptic terminals of photoreceptors and bipolar cells is thought to be a voltage-gated L-type calcium channel containing the Cav1.4 α1 subunit, which is encoded by the X-chromosomal *CACNA1F* gene. In this study, we analyzed the retinal phenotypes in Cav1.4-KO and Cav1.4 heterozygous mice and in human female carrier patients. ERG tests and behavioral test of visual performance suggest homozygous Cav1.4-KO mice are essentially blind. In these mice, a pronounced synaptopathy, characterized by retraction of rod and cone photoreceptor synapses, sprouting of second-order neurons, formation of ectopic synapses and pronounced degeneration and loss of cone, but not of rod photoreceptors were present. These findings indicate that Cav1.4 channels are essential for both rod and cone neurotransmission and the functional and structural integrity of photoreceptor synapses in mice. This conclusion is in line with results reported for a Cav1.4-KO mouse model, which was genetically independently engineered and previously characterized (13,29).

Our analysis of Cav1.4 heterozygosity in Cav1.4-KO mice revealed several new aspects of Cav1.4 channel dysfunction *in vivo*. First, they suggest that retinal function in the heterozygous Cav1.4 retina is impaired, because the affected 'knockout' retinal columns do not contribute to light detection, processing and transmission through the visual pathway (Fig. 8). The

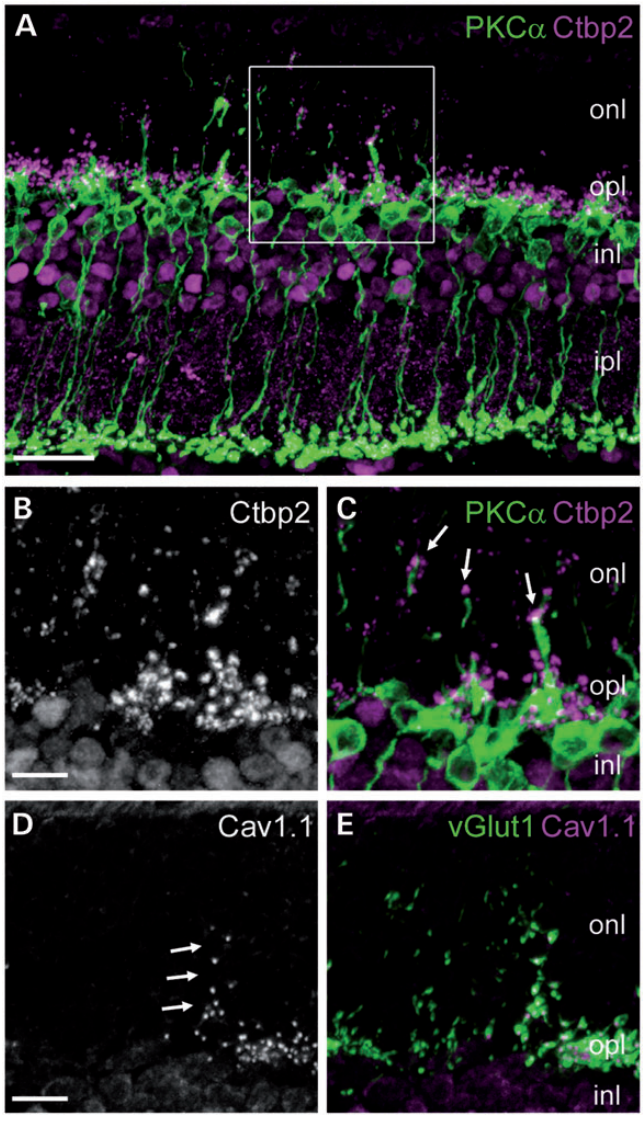

Figure 5. Pre- and postsynaptic changes in *Cacna1f* heterozygous mice. Confocal scans of vertical retinal sections from Cav1.4 heterozygous (hz) mice double-labeled for a combination of pre- and postsynaptic marker proteins. (**A**) Immunostaining for the ribbon synapse marker C-terminal binding protein 2 (Ctbp2, magenta) and PKCα (green). Ctbp2 labels ipl cell bodies as well as inl and opl synapses. In the non-affected parts the Ctbp2 signal of photoreceptor synapses is restricted to the opl. In the affected parts PKCα-positive dendrites grow into the onl and Ctbp2 is re-distributed throughout the onl. (**B** and **C**) High resolution images of the area marked with a rectangle in (A). (B) Ctbp2 (grey) signal only. (C) Merged image for Ctbp2 (magenta) and PKCα (green). The arrows mark ectopic Ctbp2-positive structures in close proximity to the tips of outgrown PKCα-positive rod bipolar cell dendrites. (**D** and **E**) Co-immunostaining for the postsynaptic L-type calcium channel subunit 1.1 (Cav1.1) and vGlut1. The arrows point to Cav1.1-positive puncta at the border of the affected area. (D) Cav1.1 signal (grey) only. (E) Merged image for Cav1.1 (magenta) and vGlut1 (green). The scale bar marks 10 μm. inl, inner nuclear layer; onl, outer nuclear layer; opl, outer plexiform layer.

prerequisite of this idea is the presence of a retinal mosaic in Cav1.4 heterozygous mice, characterized by radial retinal columns of Cav1.4-KO morphology was present in the Cav1.4-KO mouse retina side by side to radial columns of wild-type-like morphology. It is very likely that this mosaic like pattern is caused by differential X-chromosomal inactivation prior to the onset of neurogenesis (30). When the X-chromosome is inactivated in early retinal precursor cells, those cells with inactivation of the wild-type *Cacna1f*- gene would lead to cells deficient of Cav1.4 in carriers. Clonal descendents of retinal precursor cells inherit the X-active status of their ancestors and these clones are precisely organized in radial columns (30–32). Importantly, the morphological changes observed in affected columns of carrier mice included the synaptopathy as well as the degenerative changes of cone photoreceptors. Given the presence of radial Cav1.4-KO columns, it is likely that the vertical flow of visual information is compromised and cannot be compensated by neighboring unaffected and functional retinal cells.

Secondly, we provide evidence that aberrant crosstalk originating from the border areas between affected and non-affected retinal columns could interfere with normal retinal processing. In line with this hypothesis, ectopic synapses are formed between neurites originating from second order neurons within the affected retinal column and rod photoreceptor somata in non-affected columns (Fig. 8).

On a functional level, Cav1.4 heterozygous mice revealed reduced amplitudes of ERG b-waves and oscillatory potentials and a compromised performance in the vision-guided behavior which was in between that of wild-type and Cav1.4-KO mice. Notably, this phenotype was observed under scotopic and photopic light conditions arguing for defects in rod and cone function. We noticed that the phenotype of carrier mice was more pronounced at the level of vision-guided behavior than in the ERG. This might be attributable to significant disturbance of retinal network signaling in carrier mice (Fig. 8).

In humans, most X chromosomal diseases do not lead to clinical symptoms in carrier females (33). However, exceptions are retinal diseases like specific subtypes of X-linked retinitis pigmentosa (34) and Choroideremia (35). In carriers for CSNB2 associated with mutations in *CACNA1F* clinically detectable signs are relatively rare (10,17,18). Here, we present five female carriers which had decreased cone-specific ERG responses. These carriers had independent *CACNA1F* mutations, four of which were novel. From the structural point of view, it is very likely that the frameshift mutations lead to a loss of Cav1.4 function. The specific functional consequences of the two point mutations are not known. The presence of symptoms in female carrier heterozygous for different mutations in *CACNA1F* supports the hypothesis of X-inactivation. Furthermore, variable expressivity of symptoms observed in different carriers is consistent with differential X-inactivation. Finally, the observation that not all carriers in the families of a given mutation are affected suggests partial penetrance which also agrees with X-chromosomal inactivation. Together, these clinical data suggest that X-inactivation rather than a specific effect of a mutation is responsible for the specific clinical presentation of an individual carrier. Supposed the morphological changes observed in the retina of Cav1.4 heterozygous mice are also present in the human retina of Cav1.4 carrier females, one would expect impaired vertical processing of visual information in affected retinal network columns. In addition, aberrant crosstalk between affected and non-affected retinal columns would lead to erroneous visual signal processing. However, one needs to take into account that the human retina differs in many ways from the mouse retina. For instance, human daylight vision

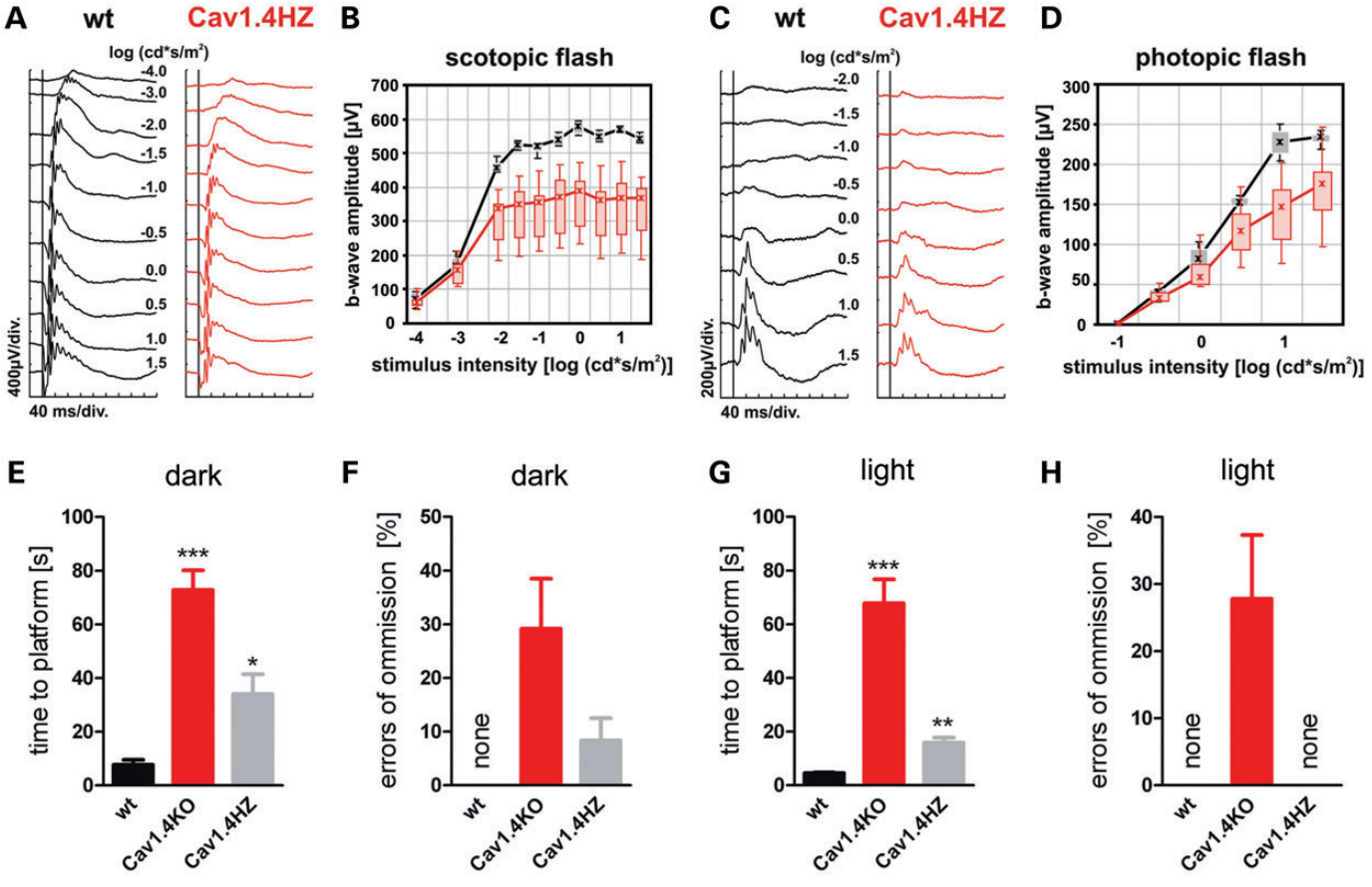

Figure 6. Visual function in *Cacna1f* heterozygous mice. (**A**–**D**) Electroretinographic analysis of retinal function in Cav1.4 HZ mice. Representative Ganzfeld-ERG intensity series from dark-adapted (A) and light-adapted (C) wild-type (wt, black traces) and Cav1.4 HZ mice (red traces). (B and D) Quantitative data of the entire group shown as Box-and-Whisker plots, i.e. boxes indicate the 25 and 75% quantile range, whiskers indicate the 5 and 95% quantiles and the asterisks indicate the median of the data. The amplitude data are plotted as a function of the logarithm of the flash intensity. (**E**–**H**) Performance of Cav1.4 HZ mice (grey) in a visual water-maze behavioral task under dark (E and F) or normal light conditions (G and H). Wild-type (wt, black) and Cav1.4-KO mice (red) are show for comparison. (E and G) Latency to locate a visible platform under dark (E) and normal light conditions (G). (F and H) Errors of ommision under dark (F) and normal light conditions (H).

mainly depends on the foveal/macular cone photoreceptors. Moreover, it is still not clear whether human cones (or rods) express other L-type VDCCs (e.g. Cav1.3) in addition to Cav1.4 that might compensate for the loss of Cav1.4 function. These reasons could at least partially explain why the phenotype in mice has such deleterious effects whereas in humans it is hardly noticed subjectively.

Our study provides the first comprehensive description of morphological and functional changes in female carriers due to mutations in *CACNA1F* affecting the Cav1.4 channel. Our data indicate that *CACNA1F* heterozygosity in female carrier mice and humans have significant consequences for both rod and cone-mediated vision and that this functional impairment is presumably caused by X-chromosomal inactivation of the wild-type Cav1.4 allele. Finally, our study helps to explain previously not understood complaints of mutant Cav1.4 carriers.

MATERIALS AND METHODS

Animals

We used Cav1.4-KO mice obtained from Dr Marion Maw, University of Otago, Dunedin, New Zealand (14). In these mice, the *Cacna1f* locus was globally disrupted through homologous recombination by a Cre/loxP-based deletion of exons 14–17 which encode the transmembrane helices 8–12 located in domain 2 of the channel protein (14). The deletion of exon 14–17 of the Cav1.4 gene was confirmed at the level of genomic DNA by Southern blot analysis (Supplementary Material, Fig. S1A and B). Cav1.4-KO mice (Cav1.4-KO) were born at the expected Mendelian ratio, were fertile and showed no immediately visible behavioral and physical abnormalities.

Immunohistochemistry

Immunohistochemical staining was performed on retinal cryosections according to the procedures described previously (21).

Briefly, after enucleation, the eyes were pierced with a needle and fixed for 5 min with 4% paraformaldehyde (PFA) in 0.1 M phosphate buffer (PB). Subsequently, the cornea and lens were removed and the remaining eye cut was fixed for 45 min in 4% PFA/PB, then washed three times in 0.1 M PB and incubated overnight in 30% sucrose/PB. After embedding in tissue freezing medium (Tissue-Tek O.C.T Compound, Sakura Finetech), vertical cryosections were cut at 10 µm and stored at −20°C until

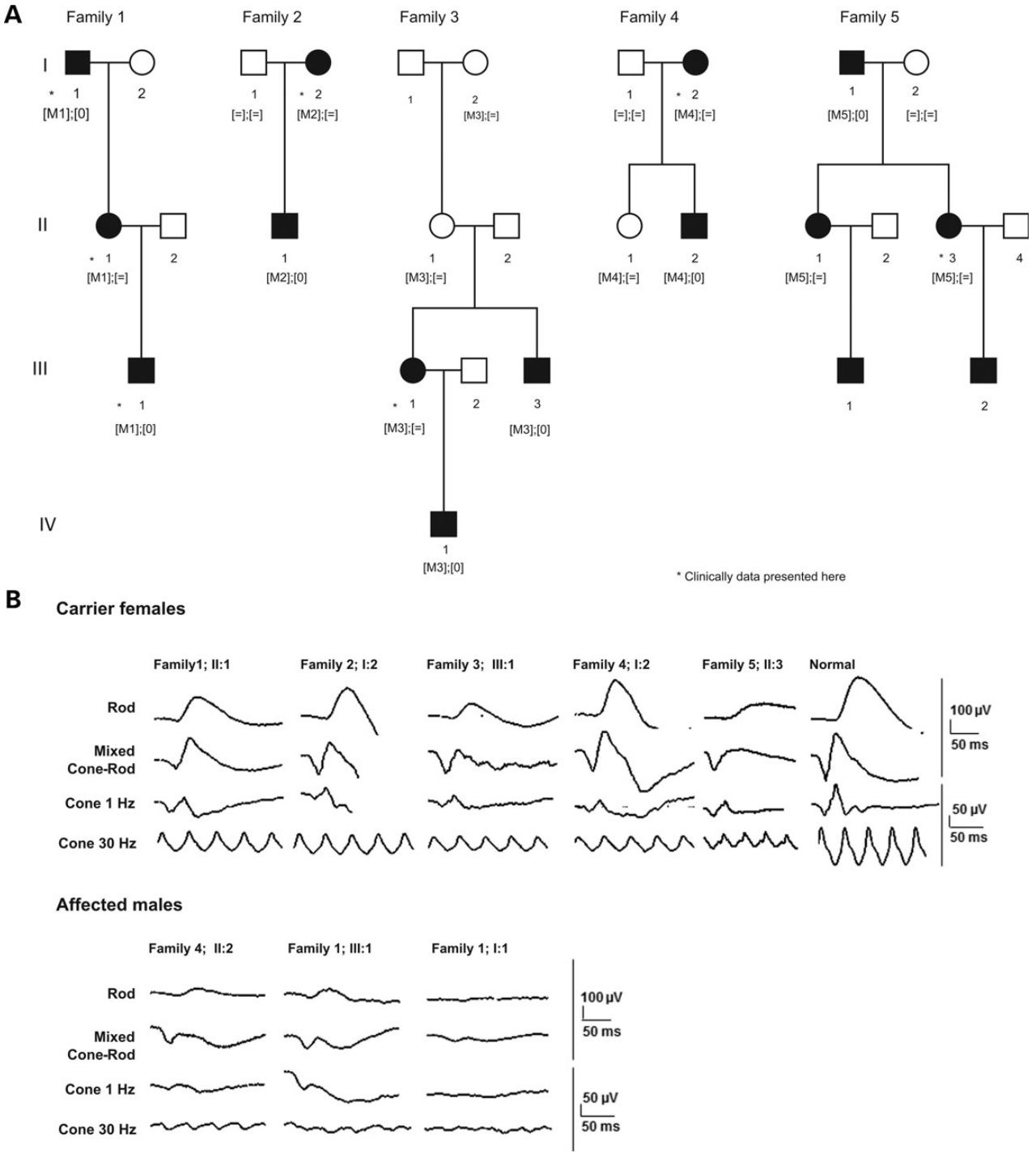

Figure 7. Visual function in human CSNB patients carrying *CACNA1F* mutations (**A**) Pedigrees of incomplete CSNB patients and carriers with *CACNA1F* mutations and co-segregation analysis in available family members. Filled symbols represent affected and unfilled unaffected individuals. Squares depict males, circles females. Stars mark individuals for whom we present the clinical data. Equation symbols represent unaffected alleles. (**B**) Electroretinograms (ERG) of carriers and male patients set-up to stimulate: I. rods (dark adapted, 0.01*cd*m^{-2}s), II. cones and rods (dark adapted, 3*cd*m^{-2} s); III. and IV. cones (light adapted, 3 cd*m^{-2} s, 1 Hz and 30 Hz). Compared with normal responses displayed in the last column, carriers had a variable *b*-wave responses under rod conditions. Those with markedly low *b*-waves (RP1214 and 1344.01) did not reach a larger *b*- than *a*-wave for the mixed cone-rod condition ('negative' ERG). Under rod suppression by light adaptation no carrier reached more than about 50% of the normal response to either single flashes (1 Hz) or flicker (30 Hz). Responses of all three affected males were much smaller under both dark and light adapted condition.

use. The retina slices were rehydrated with 0.1 M PB and then fixed for 10 min with 4% PFA. After washing three times with 0.1 M PB, the slices were incubated with primary antibody overnight at 4°C in a solution of 0.1 M PB, 5% Chemiblocker (Millipore) and 0.3% Triton X. Next, the slices were again washed three times with 0.1 M PB, before proceeding with

Table 1. Clinical details of carriers

Family number, internal reference number	CACNA1F mutation found in son	Exon/ Intron	Sex, age	History	Refractive error RE, LE	VA; RE; LE	ERG
Family 1, Mo802,	c.2821dupC => p.Leu941Pfs*115 heterozygote	Ex 23	F, 34	Strabismus in childhood, surgery, amblyopia right eye	+2.50/0.75/90° +1.25 sph	0.3* 1.0	Electronegative cone response, decreased 30-Hz flickers amplitudes, rod responses in the lower range
Family 2, Mo1189,	c.2090T>C => p.Leu697Pro heterozygote	Ex 16	F, 22	Amblyopia left eye, needs relatively strong lights	+2.50/−0.50/80° +5.00/−0.50/20°	1.0 0.7*	Electronegative cone response, decreased 30-Hz flickers amplitudes, rod responses in the normal range
Family 3, Mo1214,	c.4547_4549delinsCC => p.Leu1516Profs*9 heterozygote	Ex 39	F, 31	Refractive surgery at age 28 years for astigmatism	0/−1.25/55° −0.25/−0.25/100°	0.9 0.9	Highly electronegative cone response, half decreased 30-Hz flickers amplitudes, decreased rod responses
Family 4 Mo1242,	c.764G>A => p.Gly255Glu heterozygote	Ex 6	F, 34	—	—	—	Decreased cone response, decreased 30-Hz flickers amplitudes, rod responses in the normal range
Family 5 Gi1344.01	c.2928+1G>A => 4S24+1 heterozygote	In 24	F, 51	Photophobic for bright light	−0.25/−0.5/152° −1.75/−0.75/8°	0.7 0.7	Negative ERG: rod, mixed and cone b-waves about $\frac{1}{2}$ of normal, a-waves normal. Rod b-wave delayed.

Refractive errors (sph spherical/cylindrical diopters/and axes) and corresponding visual acuity (VA); Electroretinograms (ERGs) were all below mean normal amplitudes, latencies unchanged except for rod response Family 5; II:3. Two carriers had abnormal fundus appearance: In Family 4; I:2 the color of the peripheral retina appeared slightly heterogenous; equally, Family 5; II:3 had overall light fundus pigmentation, in the LE circular chorioretinal atrophy of one optic disc diameter (disease unrelated). In both eyes, no macular reflex was seen and optic discs were pale. This was confirmed by spectral-domain optical coherence tomography which illustrated a shallow foveal pit and partial optic atrophy with thinning of the retinal nerve fiber layer around the optic disc. Fundus autofluorescence, was slightly irregular (sparkled higher and lower FAF) around the macula, while Family 1; II:1 had a normal appearance. RE right eye; LE left eye; —, data not obtained; One carrier (Family 5; II:3) named symptoms, i.e. sensitivity to bright light. One carrier (Gi1344.01) had moderate myopia. Carriers Family 5; II:3 and Family 3; III:1 did not reach normal visual acuity despite best correcting glasses.
*Visual acuity reduced due to amblyopia in squinting eye.

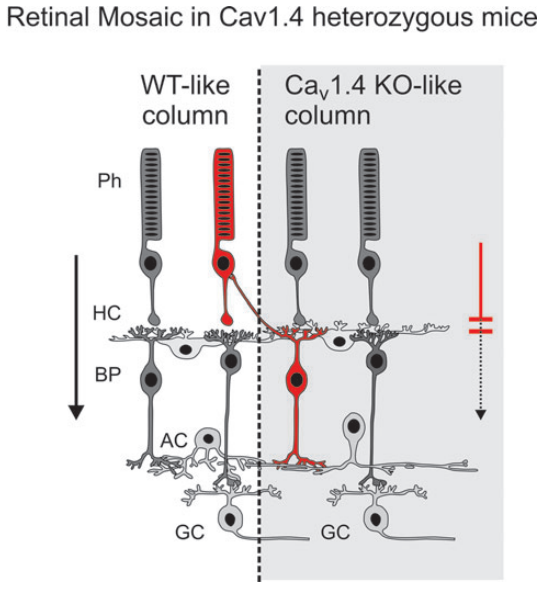

Figure 8. Model for pathological retinal information processing in Cav1.4 heterozygous mice. Retinal mosaic in Cav1.4 heterozygous mice showing a wild-type like retinal column (left part of the figure) and a Cav1.4-KO like retinal column (right part of the figure). Affected 'knockout' retinal columns do not contribute to light detection, processing and transmission through the visual pathway (arrow on the right). Aberrant crosstalk at the border areas between affected and non-affected retinal columns interfere with normal retinal processing. Formation of ectopic synapses between neurites originating from second order neurons within the affected retinal column and rod photoreceptor somata in non-affected columns (Red rod photoreceptor and red bipolar neuron). Ph, rod photoreceptor; BP, bipolar cell; GZ, ganglion cell; HZ, horizontal cell; AZ, amacrine cell.

secondary detection using Alexa 488 anti-mouse or rabbit IgG $F(ab')_2$ fragments (Cell Signaling Technology) or anti-guinea pig IgG (Mobitec) or Cy3 anti-mouse or anti-rabbit IgG (Jackson Immunoreagents). The cell nuclei were stained with Hoechst 33342. Finally, the sections were washed with 0.1 M PB and covered with coverslips.

The following primary antibodies were used: rabbit anti-Cav1.4 (Cav1.4 Pep3; 1:1000) (14), mouse anti-Cav1.1 (Millipore, clone mab1A, 1:5000), rabbit anti-calbindin (Swant, Bellinzona, Switzerland; 1:2000) (23), rabbit anti-cone arrestin (1:300) (23,36), rabbit anti-complexin 3 (1:1000) (25), rabbit anti-complexin 4 (1:20 000) (25), mouse anti-Ctbp2 (BD Biosciences, 1:10 000), Cy3-coupled anti-GFAP (Sigma, Germany; 1:1000) (21), mouse anti-PKCα (clone MC5, Leinco Technologies, Inc.; 1:50) (21), rabbit anti-PKCα; Sigma, 1:1000), mouse anti-rhodopsin (anti-rhodopsin Clone 1D4; Thermo Scientific; 1:150) (37), mouse anti-vGlut1 (NeuroMab, clone N28/9; 1:1000), guinea pig anti-vGlut1 (Millipore, 1:50 000), FITC-peanut agglutinin (PNA, Sigma-Aldrich, 1:100) (21) was used as a cone marker. Confocal images were collected at a Zeiss LSM 510 laser scanning microscope (Carl Zeiss, Germany) and images are presented as collapsed confocal z-stacks. The stainings were reproduced in ≥3 independent experiments.

Electroretinograms in mice

ERG analysis was performed according to procedures described elsewhere (38,39).

Visual water maze task

Mice were housed separately in an inverse 12 h light/dark cycle. The experiment was performed in the dark cycle. Mice were trained for 3 days (eight trials a day) to locate a stable platform (10 cm in diameter) at dim light conditions of 0.3 cd/m^2 to ensure that vision is totally conferred to the rod system. The platform was placed in a circular swimming pool (120 cm in diameter, 70 cm high, white plastic) filled with water. The starting position of the mouse was changed from trial to trial in a pseudo-random order whereas the platform was kept in a constant location. Distal cues in the testing room and the water maze, such as patterned cardboards, were provided as spatial references. Trials were terminated if the mouse climbed onto the platform or when it swam for 2 min. If the mouse did not find the platform, it was gently placed on the stable platform. After each trial, the mouse was left on the platform for 10 s undisturbed before warmed using a heating lamp and transferred to the home cage. On day 4, 5 and 6, the experiment was performed under light conditions (29 cd/m^2) to test cone vision mediated behavior. In a second experiment, we tested another group of animals for three consecutive days under normal light conditions (29 cd/m^2) only to exclude any behavioral adaptation effects on the cone function test. The experiments were performed and analyzed blindly to the animal genotype.

Mutation analysis

Total genomic DNA was extracted from peripheral leukocytes in blood samples by standard salting out procedure or according to the manufacturer's recommendation (Puregen Kit; Qiagen, Courtaboeuf, France).The 48 exons of *CACNA1F* (RefSeq: AJ006216) were amplified on 50 µl genomic DNA using 33 fragments (oligonucleotide sequences and exact conditions can be obtained on request) with a polymerase (HotFire, Solis Biodyne, Estonia). The PCR products were enzymatically purified (ExoSAP-IT, USB Corporation, Cleveland, OH, USA purchased from GE Healthcare, Orsay, France) and sequenced with a commercially available sequencing mix (BigDyeTerm v1.1 CycleSeq kit, Applied Biosystems, Courtaboeuf, France). The sequenced products were purified on a pre-soaked Sephadex G-50 (GE Healthcare) 96-well multiscreen filter plate (Millipore, Molsheim, France), the purified product analyzed on an automated 48-capillary sequencer (ABI 3730 Genetic analyzer, Applied Biosystems) and the results interpreted by applying a software (SeqScape, Applied Biosystems). At least 192 commercially available control samples were used to validate the pathogenicity of the novel sequence variants (Human random control panel 1–3, Health Protection Agency Culture Collections, Salisbury, UK).

Phenotypic characterization of patients and carriers

Patients had standard ophthalmological examination (refractometry, visual acuity, slit-lamp examination, applanation tonometry, funduscopy with pupil dilatation). Optical coherence tomography (OCT) was obtained in Montpellier using a time domain OCT (TD-OCT, Stratus model 3000, Carl Zeiss Meditec, CA, USA, software version 3.0) and in Giessen using a spectral domain OCT (SD-OCT, Spectralis, Heidelberg

Enginieering, Heidelberg, Germany). Fundus autofluorescence was imaged with a confocal laser ophthalmoskop (HRA2 in Montpellier and HRA3 in Gießen; both by Heidelberg Engineering, Heidelberg, Germany). Full-field ERGs were recorded under pupil dilatation using the MonPackOne (Metrovision, Pérenchies, France) with bipolar contact lens electrodes (Montpellier) or a ColorDome Ganzfeld stimulator with an ESPION-system and DTL-Electrodes (Diagnosys UK Ltd, Impington, Cambridge, UK) in line with recommendatations of the International Society for Clinical Electrophysiology of Vision (http ://www.iscev.org/standards/index.html).

SUPPLEMENTARY MATERIAL

Supplementary Material is available at *HMG* online.

ACKNOWLEDGEMENTS

We thank Kathrin Rötzer, Gudrun Utz and Elisabeth Schulze for excellent technical help, Drs Marion Maw (University of Otago) and Susanne tom Dieck (Max Planck Institute for Brain Research) for providing Cav1.4 KO mice and Cav1.4 antibodies and Drs Wolfgang Baehr (University of Utah) and Kerstin Reim (Max Planck Institute of Experimental Medicine, Göttingen) for the gift of antibodies. The monoclonal antibody anti-vGlut1 N28/9 was obtained by the UC Davis/NIH NeuroMab Facility.

Conflict of Interest statement. None declared.

FUNDING

This work was supported by the Deutsche Forschungsgemeinschaft (DFG) (WA 2597/2-1); Foundation *Voir et Entendre* (C.Z.), Prix Dalloz for *'la recherche en ophtalmologie*' (C.Z.), Ville de Paris and Region Ile de France, LABEX LIFESENSES (reference ANR-10-LABX-65) supported by French state funds managed by the ANR within the *Investissements d'Avenir programme* (ANR-11-IDEX-0004-0).

REFERENCES

1. Matthews, G. and Fuchs, P. (2010) The diverse roles of ribbon synapses in sensory neurotransmission. *Nat. Rev. Neurosci.*, **11**, 812–822.
2. Heidelberger, R., Thoreson, W.B. and Witkovsky, P. (2005) Synaptic transmission at retinal ribbon synapses. *Prog. Retin. Eye Res.*, **24**, 682–720.
3. Baumann, L., Gerstner, A., Zong, X., Biel, M. and Wahl-Schott, C. (2004) Functional characterization of the L-type Ca2+ channel Cav1.4alpha1 from mouse retina. *Invest Ophthalmol. Vis. Sci.*, **45**, 708–713.
4. Wahl-Schott, C., Baumann, L., Cuny, H., Eckert, C., Griessmeier, K. and Biel, M. (2006) Switching off calcium-dependent inactivation in L-type calcium channels by an autoinhibitory domain. *Proc. Natl Acad. Sci. USA*, **103**, 15657–15662.
5. McRory, J.E., Hamid, J., Doering, C.J., Garcia, E., Parker, R., Hamming, K., Chen, L., Hildebrand, M., Beedle, A.M., Feldcamp, L. *et al.* (2004) The CACNA1F gene encodes an L-type calcium channel with unique biophysical properties and tissue distribution. *J. Neurosci.*, **24**, 1707–1718.
6. Koschak, A., Reimer, D., Walter, D., Hoda, J.C., Heinzle, T., Grabner, M. and Striessnig, J. (2003) Cav1.4alpha1 subunits can form slowly inactivating dihydropyridine-sensitive L-type Ca2+ channels lacking Ca2+-dependent inactivation. *J. Neurosci.*, **23**, 6041–6049.
7. Ball, S.L., Powers, P.A., Shin, H.S., Morgans, C.W., Peachey, N.S. and Gregg, R.G. (2002) Role of the beta(2) subunit of voltage-dependent calcium channels in the retinal outer plexiform layer. *Invest. Ophthalmol. Vis. Sci.*, **43**, 1595–1603.
8. Strom, T.M., Nyakatura, G., Apfelstedt-Sylla, E., Hellebrand, H., Lorenz, B., Weber, B.H., Wutz, K., Gutwillinger, N., Ruther, K., Drescher, B. *et al.* (1998) An L-type calcium-channel gene mutated in incomplete X-linked congenital stationary night blindness. *Nat. Genet.*, **19**, 260–263.
9. Bech-Hansen, N.T., Naylor, M.J., Maybaum, T.A., Pearce, W.G., Koop, B., Fishman, G.A., Mets, M., Musarella, M.A. and Boycott, K.M. (1998) Loss-of-function mutations in a calcium-channel alpha1-subunit gene in Xp11.23 cause incomplete X-linked congenital stationary night blindness. *Nat. Genet.*, **19**, 264–267.
10. Jalkanen, R., Bech-Hansen, N.T., Tobias, R., Sankila, E.M., Mantyjarvi, M., Forsius, H., de la Chapelle, A. and Alitalo, T. (2007) A novel CACNA1F gene mutation causes Aland Island eye disease. *Invest. Ophthalmol. Vis. Sci.*, **48**, 2498–2502.
11. Vincent, A., Wright, T., Day, M.A., Westall, C.A. and Heon, E. (2011) A novel p.Gly603Arg mutation in CACNA1F causes Aland island eye disease and incomplete congenital stationary night blindness phenotypes in a family. *Mol. Vis.*, **17**, 3262–3270.
12. Jalkanen, R., Mantyjarvi, M., Tobias, R., Isosomppi, J., Sankila, E.M., Alitalo, T. and Bech-Hansen, N.T. (2006) X linked cone-rod dystrophy, CORDX3, is caused by a mutation in the CACNA1F gene. *J. Med. Genet.*, **43**, 699–704.
13. Mansergh, F., Orton, N.C., Vessey, J.P., Lalonde, M.R., Stell, W.K., Tremblay, F., Barnes, S., Rancourt, D.E. and Bech-Hansen, N.T. (2005) Mutation of the calcium channel gene Cacna1f disrupts calcium signaling, synaptic transmission and cellular organization in mouse retina. *Hum. Mol. Genet.*, **14**, 3035–3046.
14. Specht, D., Wu, S.B., Turner, P., Dearden, P., Koentgen, F., Wolfrum, U., Maw, M., Brandstatter, J.H. and tom Dieck, S. (2009) Effects of presynaptic mutations on a postsynaptic Cacna1s calcium channel colocalized with mGluR6 at mouse photoreceptor ribbon synapses. *Invest. Ophthalmol. Vis. Sci.*, **50**, 505–515.
15. Chang, B., Heckenlively, J.R., Bayley, P.R., Brecha, N.C., Davisson, M.T., Hawes, N.L., Hirano, A.A., Hurd, R.E., Ikeda, A., Johnson, B.A. *et al.* (2006) The nob2 mouse, a null mutation in Cacna1f: anatomical and functional abnormalities in the outer retina and their consequences on ganglion cell visual responses. *Vis. Neurosci.*, **23**, 11–24.
16. Doering, C.J., Rehak, R., Bonfield, S., Peloquin, J.B., Stell, W.K., Mema, S.C., Sauve, Y. and McRory, J.E. (2008) Modified Ca(v)1.4 expression in the Cacna1f(nob2) mouse due to alternative splicing of an ETn inserted in exon 2. *PLoS One*, **3**, e2538.
17. Hemara-Wahanui, A., Berjukow, S., Hope, C.I., Dearden, P.K., Wu, S.B., Wilson-Wheeler, J., Sharp, D.M., Lundon-Treweek, P., Clover, G.M., Hoda, J.C. *et al.* (2005) A CACNA1F mutation identified in an X-linked retinal disorder shifts the voltage dependence of Cav1.4 channel activation. *Proc. Natl Acad. Sci. USA*, **102**, 7553–7558.
18. Rigaudiere, F., Roux, C., Lachapelle, P., Rosolen, S.G., Bitoun, P., Gay-Duval, A. and Le Gargasson, J.F. (2003) ERGs in female carriers of incomplete congenital stationary night blindness (I-CSNB). A family report. *Doc. Ophthalmol.*, **107**, 203–212.
19. Hope, C.I., Sharp, D.M., Hemara-Wahanui, A., Sissingh, J.I., Lundon, P., Mitchell, E.A., Maw, M.A. and Clover, G.M. (2005) Clinical manifestations of a unique X-linked retinal disorder in a large New Zealand family with a novel mutation in CACNA1F, the gene responsible for CSNB2. *Clin. Exp. Ophthalmol.*, **33**, 129–136.
20. Dick, O., tom Dieck, S., Altrock, W.D., Ammermuller, J., Weiler, R., Garner, C.C., Gundelfinger, E.D. and Brandstatter, J.H. (2003) The presynaptic active zone protein bassoon is essential for photoreceptor ribbon synapse formation in the retina. *Neuron*, **37**, 775–786.
21. Huttl, S., Michalakis, S., Seeliger, M., Luo, D.G., Acar, N., Geiger, H., Hudl, K., Mader, R., Haverkamp, S., Moser, M. *et al.* (2005) Impaired channel targeting and retinal degeneration in mice lacking the cyclic nucleotide-gated channel subunit CNGB1. *J. Neurosci.*, **25**, 130–138.
22. Lewis, G.P., Linberg, K.A. and Fisher, S.K. (1998) Neurite outgrowth from bipolar and horizontal cells after experimental retinal detachment. *Invest. Ophthalmol. Vis. Sci.*, **39**, 424–434.
23. Koch, S., Sothilingam, V., Garcia Garrido, M., Tanimoto, N., Becirovic, E., Koch, F., Seide, C., Beck, S.C., Seeliger, M.W., Biel, M. *et al.* (2012) Gene therapy restores vision and delays degeneration in the CNGB1(-/-) mouse model of retinitis pigmentosa. *Hum. Mol. Genet.*, **21**, 4486–4496.

24. Haverkamp, S., Ghosh, K.K., Hirano, A.A. and Wassle, H. (2003) Immunocytochemical description of five bipolar cell types of the mouse retina. *J. Comp. Neurol.*, **455**, 463–476.
25. Landgraf, I., Muhlhans, J., Dedek, K., Reim, K., Brandstatter, J.H. and Ammermuller, J. (2012) The absence of Complexin 3 and Complexin 4 differentially impacts the ON and OFF pathways in mouse retina. *Eur. J. Neurosci.*, **36**, 2470–2481.
26. Michalakis, S., Geiger, H., Haverkamp, S., Hofmann, F., Gerstner, A. and Biel, M. (2005) Impaired opsin targeting and cone photoreceptor migration in the retina of mice lacking the cyclic nucleotide-gated channel CNGA3. *Invest. Ophthalmol. Vis. Sci.*, **46**, 1516–1524.
27. tom Dieck, S., Altrock, W.D., Kessels, M.M., Qualmann, B., Regus, H., Brauner, D., Fejtova, A., Bracko, O., Gundelfinger, E.D. and Brandstatter, J.H. (2005) Molecular dissection of the photoreceptor ribbon synapse: physical interaction of Bassoon and RIBEYE is essential for the assembly of the ribbon complex. *J. Cell Biol.*, **168**, 825–836.
28. Boycott, K.M., Maybaum, T.A., Naylor, M.J., Weleber, R.G., Robitaille, J., Miyake, Y., Bergen, A.A., Pierpont, M.E., Pearce, W.G. and Bech-Hansen, N.T. (2001) A summary of 20 CACNA1F mutations identified in 36 families with incomplete X-linked congenital stationary night blindness, and characterization of splice variants. *Hum. Genet.*, **108**, 91–97.
29. Raven, M.A., Orton, N.C., Nassar, H., Williams, G.A., Stell, W.K., Jacobs, G.H., Bech-Hansen, N.T. and Reese, B.E. (2008) Early afferent signaling in the outer plexiform layer regulates development of horizontal cell morphology. *J. Comp. Neurol.*, **506**, 745–758.
30. Reese, B.E. and Galli-Resta, L. (2002) The role of tangential dispersion in retinal mosaic formation. *Prog. Retin. Eye Res.*, **21**, 153–168.
31. Reese, B.E., Harvey, A.R. and Tan, S.S. (1995) Radial and tangential dispersion patterns in the mouse retina are cell-class specific. *Proc. Natl Acad. Sci. USA*, **92**, 2494–2498.
32. Reese, B.E. and Tan, S.S. (1998) Clonal boundary analysis in the developing retina using X-inactivation transgenic mosaic mice. *Semin. Cell Dev. Biol.*, **9**, 285–292.
33. Migeon, B.R. (2006) The role of X inactivation and cellular mosaicism in women's health and sex-specific diseases. *JAMA*, **295**, 1428–1433.
34. Wegscheider, E., Preising, M.N. and Lorenz, B. (2004) Fundus autofluorescence in carriers of X-linked recessive retinitis pigmentosa associated with mutations in RPGR, and correlation with electrophysiological and psychophysical data. *Graefes Arch. Clin. Exp. Ophthalmol.*, **242**, 501–511.
35. Preising, M.N., Wegscheider, E., Friedburg, C., Poloschek, C.M., Wabbels, B.K. and Lorenz, B. (2009) Fundus autofluorescence in carriers of choroideremia and correlation with electrophysiologic and psychophysical data. *Ophthalmology*, **116**, 1201. –1209 e1201–1202.
36. Zhang, T., Baehr, W. and Fu, Y. (2012) Chemical chaperone TUDCA preserves cone photoreceptors in a mouse model of Leber congenital amaurosis. *Invest. Ophthalmol. Vis. Sci.*, **53**, 3349–3356.
37. Molday, R.S. and MacKenzie, D. (1983) Monoclonal antibodies to rhodopsin: characterization, cross-reactivity, and application as structural probes. *Biochemistry*, **22**, 653–660.
38. Seeliger, M.W., Grimm, C., Stahlberg, F., Friedburg, C., Jaissle, G., Zrenner, E., Guo, H., Reme, C.E., Humphries, P., Hofmann, F. *et al.* (2001) New views on RPE65 deficiency: the rod system is the source of vision in a mouse model of Leber congenital amaurosis. *Nat. Genet.*, **29**, 70–74.
39. Tanimoto, N., Muehlfriedel, R.L., Fischer, M.D., Fahl, E., Humphries, P., Biel, M. and Seeliger, M.W. (2009) Vision tests in the mouse: Functional phenotyping with electroretinography. *Front. Biosci. (Landmark Ed)*, **14**, 2730–2737.